INL/JOU-18-45154-Revision-0

Bond-Associated Deformation Gradients for Peridynamic Correspondence Model

Hailong Chen

April 2018

The INL is a U.S. Department of Energy National Laboratory
operated by Battelle Energy Alliance

INL/JOU-18-45154-Revision-0

Bond-Associated Deformation Gradients for Peridynamic Correspondence Model

Hailong Chen

April 2018

Idaho National Laboratory
Idaho Falls, Idaho 83415

http://www.inl.gov

Prepared for the
U.S. Department of Energy
Office of Nuclear Energy
Under DOE Idaho Operations Office
Contract DE-AC07-05ID14517

Bond-Associated Deformation Gradients for Peridynamic Correspondence Model

Hailong Chen*

Fuels Modeling and Simulation Department, Idaho National Laboratory, Idaho Falls, ID 83402

Abstract

Non-ordinary state-based peridynamic correspondence material model is known to have issues with material instability, i.e. the existence of zero-energy modes, due to non-unique mapping between deformation states and force states via the conventional peridynamic deformation gradient. In this paper, an alternative approach in which the deformation gradient hence force state are computed specifically for each individual bond is proposed to eliminate the material instability. Bond-associated deformation gradient is calculated based on deformation states of material points within an individual bond's proximity, termed here as the bond-associated family, rather than a material point's whole family. This bond-associated deformation gradient can better represent the force state of each individual bond from the deformation states of material points in its proximity, and hence inherently resolves issues of material instability in the conventional correspondence material model. Parametric study on bond-associated horizon size indicates that the optimal size should be no less than the material point's horizon size but smaller than two times of that value. Comparisons against reference solutions using finite element method establish the validity and accuracy of the proposed formulation.

Keywords: Peridynamics; State-based Peridynamics; Correspondence model; Stability; Zero-energy modes; Deformation gradient

* *Tel.*: +1 208 526 2542.
E-mail address: hailong.chen@inl.gov.

1. Introduction

Among peridynamic models [1], the correspondence model [2] is very useful in that it allows the direct use of classical continuum material constitutive models within peridynamic theory. Continuum material models are naturally incorporated into the peridynamic framework via the counterpart measures, such as deformation gradient and first Piola-Kirchhoff stress tensor. However, the correspondence model suffers from some practical difficulties, such as non-invertibility [3]. This non-invertibility is a manifestation of material instability rather than merely an artifact of meshless discretization. It can be understood as existence of many possible deformations of a family that result in the same force state. As a consequence, there could be many possible deformation states of the entire body for a given loading. This has the practical effect of introducing zero-energy deformation modes to the model that need to be suppressed. Various remedies for zero-energy mode control are available in the literature, such as fictitious spring-force based methods [4], [5] and stabilized field state based methods [6], [7], [8], [3]. Although can be used to alleviate instabilities arising from zero-energy modes, these methods have their own issues and limitations, such as tedious parameter tuning and problematic stress oscillation. Most importantly, these methods do not provide resolution to the fundamental problem in the correspondence formulation leading to these zero-energy modes.

To fully take advantage of correspondence model in direct incorporation of continuum material constitutive relationships for nonlinear deformation and fracture modeling, there is still a strong need for effective zero-energy control schemes to be developed. In this paper, bond-associated deformation gradients are proposed to stabilize the conventional correspondence formulation to inherently resolve its material instability issue. This paper is organized as follows: Section 2 gives details on various deformation gradient definitions in both continuum theory and peridynamic theory. Following this, derivation of force state based on the proposed bond-associated deformation gradient is presented in Section 3. In Section 4, parametric study to obtain optimal bond-associated horizon size is performed. Discussions and conclusions are drawn in Section 5.

2. Deformation gradient

2.1. *Deformation gradient in continuum mechanics*

The deformation gradient is the fundamental measure of deformation in continuum mechanics. It maps line segments in the reference configuration into line segments (consisting of the same material points) in the current configuration.

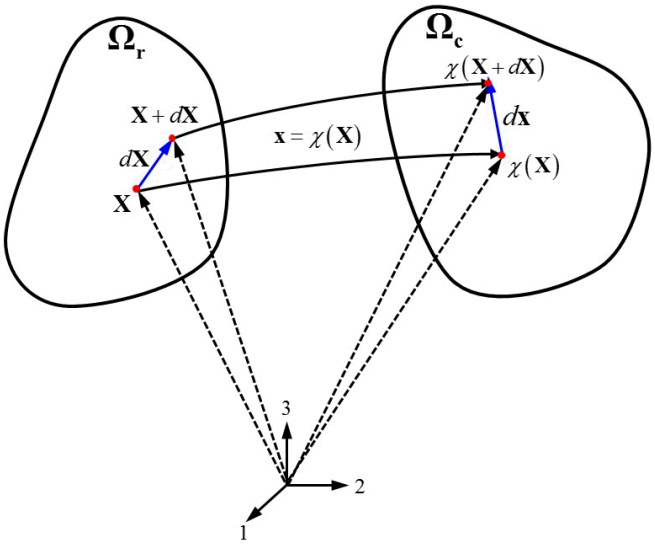

Fig. 1. Deformation of a continuum body

Consider a line segment $d\mathbf{X}$ emanating from position $\mathbf{X}$ in the reference configuration Ω_r which deforms to $d\mathbf{x}$ in the current configuration Ω_c, see Fig. 1. Thus, the line segment in the deformed configuration Ω_c is given by

$$d\mathbf{x} = \chi(\mathbf{X}+d\mathbf{X}) - \chi(\mathbf{X}) \tag{1}$$

A Taylor expansion of $\chi(\mathbf{X}+d\mathbf{X})$ gives

$$\chi(\mathbf{X}+d\mathbf{X}) = \chi(\mathbf{X}) + \frac{\partial\chi}{\partial\mathbf{X}}(\mathbf{X})\cdot d\mathbf{X} + O(d\mathbf{X}) \tag{2}$$

where $O(d\mathbf{X})$ indicates higher-order terms of $d\mathbf{X}$.

Substituting Eqn. (2) into Eqn. (1) and assuming that $|d\mathbf{X}|$ is a infinitesimally small gives

$$d\mathbf{x} \approx \frac{\partial\chi}{\partial\mathbf{X}}(\mathbf{X})\cdot d\mathbf{X} \equiv \mathbf{F}(\mathbf{X})\cdot d\mathbf{X} \tag{3}$$

Eqn. (3) tends to exact as the differential $d\mathbf{X}$ goes to zero.

The deformation gradient thus characterizes the deformation in the neighborhood of material point $\mathbf{X}$, mapping infinitesimal line segment $d\mathbf{X}$ emanating from $\mathbf{X}$ in the reference configuration to the infinitesimal line segment $d\mathbf{x}$ emanating from $\mathbf{x}$ in the deformed configuration.

2.2. Conventional peridynamic deformation gradient

Before formulating the peridynamic deformation gradient, some useful states represented in Fig. 2 are discussed below:

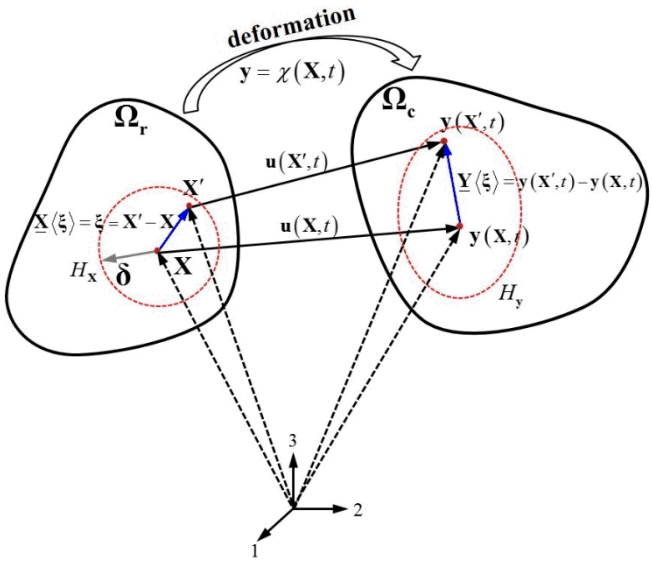

Fig. 2. Schematic illustrating different states in peridynamics

The *relative position vector state* of two material points in reference configuration Ω_r:

$$\underline{\mathbf{X}}\langle\xi\rangle = \xi = \mathbf{X}' - \mathbf{X} \tag{4}$$

where the angle bracket notation indicates that the state is associated with bond ξ.

The *relative displacement vector state* of two material points:

$$\underline{\mathbf{U}}[\mathbf{X},t]\langle\xi\rangle = \eta = \mathbf{u}(\mathbf{X}',t) - \mathbf{u}(\mathbf{X},t) \tag{5}$$

where the square bracket notation has similar meaning to standard parentheses, indicating dependence on quantities, but is used for peridynamic states.

The *relative position vector state* or *deformation state* of two material points in the current configuration Ω_c:

$$\underline{\mathbf{Y}}[\mathbf{X},t]\langle\xi\rangle = \xi + \eta = \mathbf{y}(\mathbf{X}',t) - \mathbf{y}(\mathbf{X},t) \tag{6}$$

A finite distance that defines interactions between material points is called *horizon*. $H_\mathbf{X}$ denotes the horizon at material point $\mathbf{X}$ with radius δ. For regular spatial discretization, the horizon size δ is usually represented in terms of mesh spacing Δx using a spacing factor m as

$$\delta = m \cdot \Delta x \tag{7}$$

For a bond ξ, there exists infinitely many mappings that transform the relative position vector state $\underline{\mathbf{X}}\langle\xi\rangle$ in the reference configuration to the relative position vector state $\underline{\mathbf{Y}}\langle\xi\rangle$ in the current configuration. A possible transformation can be written as:

$$\underline{\mathbf{Y}}\langle\xi\rangle = \mathbf{F}_\xi \cdot \underline{\mathbf{X}}\langle\xi\rangle \tag{8}$$

where $\mathbf{F}_\xi$ is the deformation gradient for bond ξ connecting material point $\mathbf{X}$ and its neighboring material point $\mathbf{X}'$. Here, Eqn. (8) defines the operation of a peridynamic deformation gradient in a manner analogous to the continuum deformation gradient in that it maps a vector state in the reference configuration to a vector state in the current configuration. $\mathbf{F}_\xi$ becomes the deformation gradient at material point $\mathbf{X}$ when bond ξ tends to an infinitesimal length.

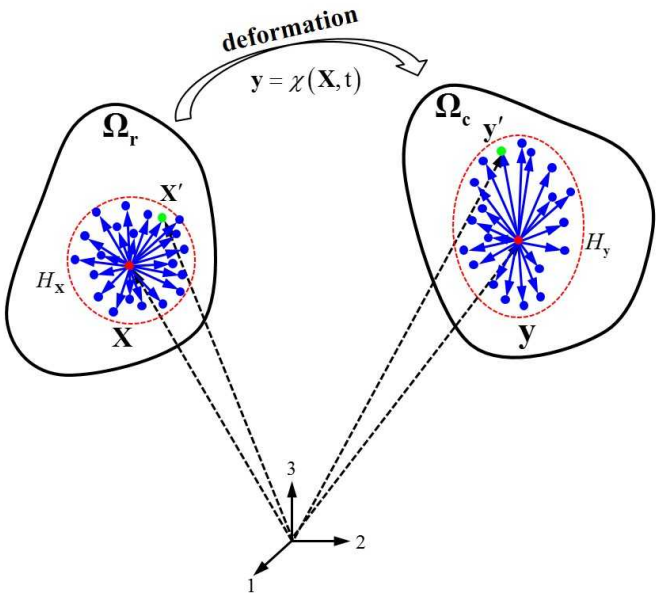

Fig. 3. Configuration for conventional peridynamic deformation gradient

Writing Eqn. (8) for material point $\mathbf{X}$ and each of the bonds connecting it with its neighbors leads to a system of over-constrained linear equations that cannot generally satisfied by a single mapping $\mathbf{F}_\xi$. See Fig. 3 for reference. For this reason, a technique to compute an optimal deformation gradient $\mathbf{F}$ is sought. Techniques similar to those discussed here have been used in molecular dynamics simulations [9] [10].

The mapping error between material point $\mathbf{X}$ and a single neighbor $\mathbf{X}'$ as the ℓ^2 norm of the difference between the $\underline{\mathbf{Y}}\langle\xi\rangle$ and $\underline{\mathbf{X}}\langle\xi\rangle$:

$$\ell_{\mathbf{X}'} = \left(\underline{\mathbf{Y}}\langle\xi\rangle - \mathbf{F}\cdot\underline{\mathbf{X}}\langle\xi\rangle\right)^T \left(\underline{\mathbf{Y}}\langle\xi\rangle - \mathbf{F}\cdot\underline{\mathbf{X}}\langle\xi\rangle\right) \tag{9}$$

Thus, the weighted least squares error among the neighbors of $\mathbf{X}$ can be given by

$$\ell = \int_{H_\mathbf{X}} \omega\langle\xi\rangle \left(\underline{\mathbf{Y}}\langle\xi\rangle - \mathbf{F}\cdot\underline{\mathbf{X}}\langle\xi\rangle\right)^T \left(\underline{\mathbf{Y}}\langle\xi\rangle - \mathbf{F}\cdot\underline{\mathbf{X}}\langle\xi\rangle\right) dV_{\mathbf{X}'} \tag{10}$$

where $\omega\langle\xi\rangle$ is a nonnegative weight factor for bond ξ.

In Eqn. (10), the volume integral has been used to arrive at a weighted least squares error. This is consistent with the volume integral in the governing equation shown in Eqn. (30) for force density.

The optimal local deformation gradient $\mathbf{F}$, in a weighted least squares sense, is obtained by minimizing ℓ in Eqn. (10) with respect to the components of $\mathbf{F}$ as

$$\frac{\partial \ell}{\partial \mathbf{F}} = \int_{H_\mathbf{X}} \omega\langle\xi\rangle \left(-2\underline{\mathbf{Y}}\langle\xi\rangle \otimes \underline{\mathbf{X}}\langle\xi\rangle + 2\mathbf{F}\cdot\underline{\mathbf{X}}\langle\xi\rangle \otimes \underline{\mathbf{X}}\langle\xi\rangle\right) dV_{\mathbf{X}'} \tag{11}$$

Setting Eqn. (11) equal to zero yields the local deformation gradient in the weighted least squares sense as

$$\mathbf{F} = \mathbf{K}_c \cdot \mathbf{K}_r^{-1} \tag{12}$$

where

$$\mathbf{K}_r = \int_{H_\mathbf{X}} \omega\langle\xi\rangle \underline{\mathbf{X}}\langle\xi\rangle \otimes \underline{\mathbf{X}}\langle\xi\rangle dV_{\mathbf{X}'} \tag{13}$$

and

$$\mathbf{K}_c = \int_{H_x} \omega\langle\boldsymbol{\xi}\rangle \underline{\mathbf{Y}}\langle\boldsymbol{\xi}\rangle \otimes \underline{\mathbf{X}}\langle\boldsymbol{\xi}\rangle dV_{\mathbf{X}'} \tag{14}$$

For Eqns. (12) - (14) to be valid, a few necessary conditions must be satisfied in cases of three-dimensional analysis. First, for $\mathbf{K}_r$ to be invertible, a material point's neighbors should not be coplanar. Second, since the deformation gradient has nine independent components, a material point must have at least three neighbors. And similar constraints apply to two-dimensional cases. Given all these conditions, the term in Eqn. (13) can be proven to be symmetric positive-definite (refer to Lemma 3.1 in [2]).

It should be noted that the above derived deformation gradient for peridynamics is different from its continuum mechanics counterpart in that it doesn't require smooth motion of a continuous region in space and it is not a continuous function of spatial position, but instead is defined only at material point locations. The compatibility condition, i.e., that the curl of the deformation gradient is zero, is usually not satisfied by the deformation gradient in peridynamics.

In the work by Silling et al. [2], the term defined in Eqn. (13) is called the *shape tensor* and denoted as $\mathbf{K}$. The notation from Ref. [2] for the shape tensor is adopted in the following discussion.

2.3 Proposed bond-associated deformation gradient

As discussed in the Introduction, the existence of zero-energy modes in correspondence model is rooted in the approximation of the nodal deformation gradient. Thus, one possible way to remove zero-energy modes at their source is to redefine the nodal deformation gradient such that there is a unique mapping between the deformation gradient and the underlying deformation states.

Based on how the conventional peridynamic deformation gradient is constructed in Section 2.2, it's obvious that an optimal peridynamic deformation gradient at a material point cannot accurately reflect the deformation of every bond associated with that material point. As a consequence, the force state calculated from this deformation gradient differs from the actual force state of each individual bond. This can sometimes lead to severe unphysical issues in peridynamic modeling, such as sub-horizon material collapse and material penetration [7]. The use of a bond-associated deformation gradient, defined below, is proposed to remedy these unphysical issues inherent in the conventional correspondence model.

According to Eqn. (8), the deformation gradient $\mathbf{F}_\xi$ can accurately capture the deformation of bond $\boldsymbol{\xi}$. However, forming this full deformation gradient is problematic because it has more components than there are constraints in a bond. In the case of three dimensions, there are nine independent components for the deformation gradient $\mathbf{F}_\xi$, and only three independent constraints are available based on the reference and current configurations of bond $\boldsymbol{\xi}$. One possible way to introduce more constraints but not change the solution such that mapped deformation of bond $\boldsymbol{\xi}$ differs significantly from the actual solution is to also use the deformation state of neighboring bonds. It is proposed that this be done by using an additional local bond-associated horizon $h_{\mathbf{X}'}$ defined at material point $\mathbf{X}'$ as shown in Fig. 4. The set of material points within this horizon that are neighbors of material point $\mathbf{X}$ is used to approximate a bond-associated deformation gradient for bond $\boldsymbol{\xi}$ at material point $\mathbf{X}$. The same methodology can be applied while calculating the bond-associated deformation gradient for bond $-\boldsymbol{\xi}$ at material point $\mathbf{X}'$. This approximated bond-associated deformation gradient is more optimal for bond deformation mapping compared to the nodal deformation gradient, since only the deformation states adjacent to this bond is used in the approximation process and the force state calculation.

The same necessary conditions listed in Section 2.2 for the approximation of the conventional peridynamic deformation gradient and shape tensor apply to the bond-associated deformation gradient and shape tensor will be derived in this section.

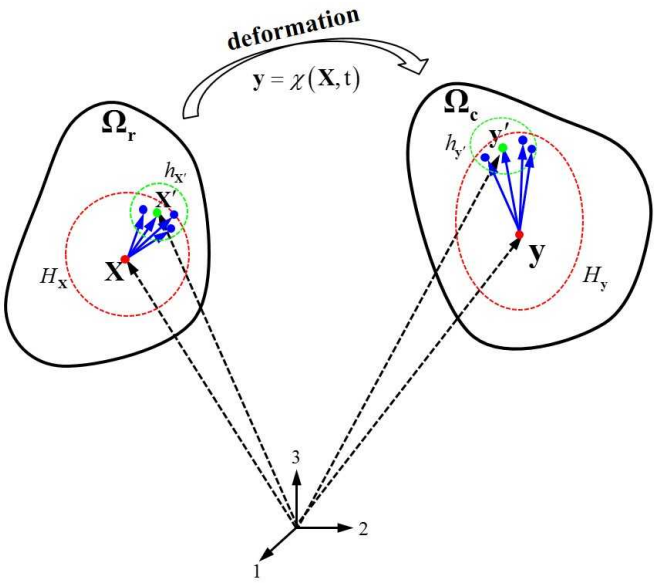

Fig. 4. Configuration for bond-associated deformation gradient

Following the same definition of conventional peridynamic deformation gradient in Eqn. (12) but using a different domain $H_{\mathbf{X}} \cap h_{\mathbf{X}'}$ rather than $H_{\mathbf{X}}$ for its weighted least squares approximation, the bond-associated deformation gradient for bond $\boldsymbol{\xi}$ at material point $\mathbf{X}$ can be readily obtained as

$$\mathbf{F}_\xi = \left(\int_{H_{\mathbf{X}} \cap h_{\mathbf{X}'}} \omega\langle\boldsymbol{\zeta}\rangle \underline{\mathbf{Y}}\langle\boldsymbol{\zeta}\rangle \otimes \underline{\mathbf{X}}\langle\boldsymbol{\zeta}\rangle dV_{\mathbf{X}'} \right) \cdot \mathbf{K}_\xi^{-1} \tag{15}$$

with the bond-associated shape tensor as

$$\mathbf{K}_\xi = \int_{H_{\mathbf{X}} \cap h_{\mathbf{X}'}} \omega\langle\boldsymbol{\zeta}\rangle \underline{\mathbf{X}}\langle\boldsymbol{\zeta}\rangle \otimes \underline{\mathbf{X}}\langle\boldsymbol{\zeta}\rangle dV_{\mathbf{X}'} \tag{16}$$

The nodal deformation gradient can be calculated as a weighted average of the bond-associated deformation gradients in Eqn. (15) for each individual bond,

$$\overline{\mathbf{F}} = \frac{\sum_{n=1}^{NP} w\langle\boldsymbol{\xi}_n\rangle \mathbf{F}_{\xi_n}}{\sum_{n=1}^{NP} w\langle\boldsymbol{\xi}_n\rangle} \tag{17}$$

where NP is the number of neighboring material points in a material points family, and the weight function $w\langle\boldsymbol{\xi}_n\rangle$ determines the contribution of each individual bond-associated deformation gradient to the deformation gradient at a material point.

It is noteworthy that the derived bond-associated deformation gradient for each individual bond becomes exact as the nodal deformation gradient when the bond approaches an infinitesimal length. This can be concluded from the definition of the continuous deformation gradient outlined in Section 2.1. In addition, for homogeneously applied deformation $\mathbf{F}_0$, this bond-associated deformation gradient is exactly the same as the applied deformation gradient as

$$\begin{aligned}\mathbf{F}_{\underline{\xi}_n} &= \int_{H_{\mathbf{X}}\cap h_{\mathbf{X}'}} \omega\langle\boldsymbol{\xi}_n\rangle\left(\mathbf{F}_0\cdot\underline{\mathbf{X}}\langle\boldsymbol{\xi}_n\rangle\right)\otimes\underline{\mathbf{X}}\langle\boldsymbol{\xi}_n\rangle\, dV_{\mathbf{X}'}\cdot\mathbf{K}_{\underline{\xi}_n}^{-1}\\ &= \mathbf{F}_0\cdot\int_{H_{\mathbf{X}}\cap h_{\mathbf{X}'}} \omega\langle\boldsymbol{\xi}_n\rangle\,\underline{\mathbf{X}}\langle\boldsymbol{\xi}_n\rangle\otimes\underline{\mathbf{X}}\langle\boldsymbol{\xi}_n\rangle\, dV_{\mathbf{X}'}\cdot\mathbf{K}_{\underline{\xi}_n}^{-1}\\ &= \mathbf{F}_0\end{aligned} \tag{18}$$

The bond-associated deformation gradient shown in Eqn. (17) aims to represents the deformation of each individual bond more accurately. This shares some similarities with the stabilization scheme recently proposed by Silling in Ref. [3].

3. Force state in bond-associated correspondence formulation

From the derivation of force state in correspondence model outlined in Ref. [2], it is clear that calculation of force state is completely dependent on the formation of deformation gradient. Differing definitions of deformation gradient will result in differing force states. Based on the proposed bond-associated deformation gradient concept, two options are possible to formulate corresponding force state. The first option is to derive the force state based on the nodal deformation gradient as is done in the classical peridynamic correspondence material model, but using the nodal deformation gradient approximated in Eqn. (17) from the bond-associated deformation gradient. A second option is to derive bond-associated force state based on each individual bond-associated deformation gradient. This will results in a set of strain energy densities at each material point, with unique values corresponding to a material point's individual neighbors, i.e., bonds connected at this materials point. This requires modification of the strain energy density definition.

In this work, focus is placed on the latter option because its implementation is much simpler. For this case, the corresponding force state can be derived following the procedure outlined in Ref. [2]. Here, focus will be placed on the modification of the strain energy density definition from material point to each individual bond connected at that material point. Details on the derivation of force state from deformation gradient can be found in Ref. [2].

At a material point, the bond-associated strain energy density function change $\Delta_{\Delta\underline{\mathbf{Y}}}W_\xi\left(\underline{\mathbf{Y}}\right)$ due to an increment $\Delta\underline{\mathbf{Y}}$ within its proximity can be determined as

$$\Delta_{\Delta\underline{\mathbf{Y}}}W_\xi\left(\underline{\mathbf{Y}}\right) = \int_{H_{\mathbf{X}}\cap h_{\mathbf{X}'}} \underline{\mathbf{T}}_\xi\left(\underline{\mathbf{Y}}\right)\cdot\Delta\underline{\mathbf{Y}}\, dV_{\mathbf{X}'} \tag{19}$$

where $\underline{\mathbf{T}}_\xi\left(\underline{\mathbf{Y}}\right)$ is the bond-associated force state.

On the other hand, the incremental change $\Delta_{\Delta\underline{\mathbf{Y}}}W_\xi\left(\underline{\mathbf{Y}}\right)$ at a material point due to an incremental change in deformation state $\underline{\mathbf{Y}}$ within a bond's proximity can also be determined as

$$\Delta_{\Delta\underline{\mathbf{Y}}}W_\xi\left(\underline{\mathbf{Y}}\right) = \frac{\partial W_\xi\left(\underline{\mathbf{Y}}\right)}{\partial\mathbf{F}_\xi\left(\underline{\mathbf{Y}}\right)} : \Delta_{\Delta\underline{\mathbf{Y}}}\mathbf{F}_\xi\left(\underline{\mathbf{Y}}\right) \tag{20}$$

The incremental change in the bond-associated deformation gradient $\Delta_{\Delta\underline{\mathbf{Y}}}\mathbf{F}_\xi$ is evaluated as

$$\begin{aligned}\Delta_{\Delta\underline{\mathbf{Y}}}\mathbf{F}_\xi\left(\underline{\mathbf{Y}}\right) &= \mathbf{F}_\xi\left(\underline{\mathbf{Y}}+\Delta\underline{\mathbf{Y}}\right)-\mathbf{F}_\xi\left(\underline{\mathbf{Y}}\right)\\ &= \int_{H_{\mathbf{X}}\cap h_{\mathbf{X}'}} \omega\langle\boldsymbol{\xi}\rangle\left(\underline{\mathbf{Y}}+\Delta\underline{\mathbf{Y}}\right)\otimes\underline{\mathbf{X}}\, dV_\xi\cdot\mathbf{K}_\xi^{-1}\\ &\quad-\int_{H_{\mathbf{X}}\cap h_{\mathbf{X}'}} \omega\langle\boldsymbol{\xi}\rangle\,\underline{\mathbf{Y}}\otimes\underline{\mathbf{X}}\, dV_\xi\cdot\mathbf{K}_\xi^{-1}\\ &= \int_{H_{\mathbf{X}}\cap h_{\mathbf{X}'}} \omega\langle\boldsymbol{\xi}\rangle\,\Delta\underline{\mathbf{Y}}\otimes\underline{\mathbf{X}}\, dV_\xi\cdot\mathbf{K}_\xi^{-1}\end{aligned} \tag{21}$$

The bond-associated first Piola-Kirchhoff stress tensor is

$$\mathbf{P}_\xi \equiv \frac{\partial W_\xi\left(\underline{\mathbf{Y}}\right)}{\partial\mathbf{F}_\xi\left(\underline{\mathbf{Y}}\right)} \tag{22}$$

From Eqns. (20)-(22), the incremental change $\Delta_{\Delta\underline{\mathbf{Y}}}W_\xi\left(\underline{\mathbf{Y}}\right)$ at a material point for an associated bond can be rewritten as

$$\Delta_{\Delta\underline{\mathbf{Y}}}W_\xi\left(\underline{\mathbf{Y}}\right) = \int_{H_{\mathbf{X}}\cap h_{\mathbf{X}}} \omega\langle\boldsymbol{\xi}\rangle\,\mathbf{P}_\xi\cdot\mathbf{K}_\xi^{-1}\cdot\underline{\mathbf{X}}\cdot\Delta\underline{\mathbf{Y}}\, dV_\xi \tag{23}$$

Comparing Eqn. (19) with Eqn. (23), the bond-associated force state $\underline{\mathbf{T}}_\xi\left[\mathbf{X},t\right]\langle\boldsymbol{\xi}\rangle$ can be obtained as

$$\underline{\mathbf{T}}_\xi\left[\mathbf{X},t\right]\langle\boldsymbol{\xi}\rangle = \omega\langle\boldsymbol{\xi}\rangle\,\mathbf{P}_\xi\cdot\mathbf{K}_\xi^{-1}\cdot\underline{\mathbf{X}} \tag{24}$$

Since the conventional correspondence formulation is based on a material point and its horizon and only a fraction of a material point and its horizon is used in the proposed bond-associated formulation, a correction is required in order to accurately represent the strain energy density at a material point from the bond-associated strain energy density at the same material point. This will eventually results in a correction factor for the force stated derived in Eqn. (24). A good approximation of the bond-associated strain energy density from the nodal strain energy density based on the volume fraction is

$$W_\xi\left(\underline{\mathbf{Y}}\right) = f_{\Sigma np/NP}\cdot W\left(\underline{\mathbf{Y}}\right)\cdot f_{np/\Sigma np} \tag{25}$$

with the volume fraction $f_{\Sigma np/NP}$ being the ratio of the total volume for all bond-associated deformation gradients at a material point with respect to that of the classical deformation gradient calculation:

$$f_{\Sigma np/NP} = \frac{\sum_{n=1}^{NP}\int_{H_{\mathbf{X}}\cap h_{\mathbf{X}_n}} 1\, dV_{\mathbf{X}'}}{\int_{H_{\mathbf{X}}} 1\, dV_{\mathbf{X}'}} \tag{26}$$

and the volume fraction $f_{np/\Sigma np}$ being the ratio of the volume used in an individual bond-associated deformation gradient calculation to the total volume for all bond-associated deformation gradients at a material point:

$$f_{np/\sum np} = \frac{\int_{H_{\mathbf{X}} \cap h_{\mathbf{x}_\xi}} 1 dV_{\mathbf{X}'}}{\sum_{n=1}^{NP} \int_{H_{\mathbf{X}} \cap h_{\mathbf{x}_n}} 1 dV_{\mathbf{X}'}} \tag{27}$$

In above Eqns. (25)-(27), np is the number of neighboring material points in a bond's proximity, i.e., bond-associated horizon.

Substituting Eqns. (26) and (27) into Eqn. (25), a simplified approximation can be obtained as

$$\underline{W}_\xi\left(\underline{\mathbf{Y}}\right) = \frac{\int_{H_{\mathbf{X}} \cap h_{\mathbf{x}_\xi}} 1 dV_{\mathbf{X}'}}{\int_{H_{\mathbf{X}}} 1 dV_{\mathbf{X}'}} \cdot \underline{W}\left(\underline{\mathbf{Y}}\right) \tag{28}$$

Thus, the force state for each individual bond in the proposed bond-associated correspondence formulation becomes

$$\underline{\mathbf{T}}\left[\mathbf{X}, t\right]\langle\xi\rangle = \frac{\int_{H_{\mathbf{X}} \cap h_{\mathbf{x}_\xi}} 1 dV_{\mathbf{X}'}}{\int_{H_{\mathbf{X}}} 1 dV_{\mathbf{X}'}} \omega\langle\xi\rangle \mathbf{P}_\xi \cdot \mathbf{K}_\xi^{-1} \cdot \underline{\mathbf{X}} \tag{29}$$

In the conventional formulation of deformation gradient (Eqn. (12)), a variation of the deformation state of any material points within the family will result in a change to the deformation gradient hence the force state of all bonds connected at the that material point. In the proposed bond-associated formulations, however, a variation in the deformation state of a material point within a bond's proximity will only affect the force state of adjacent bonds whose associated deformation gradient depends on that variation. This effectively reduces the non-locality of the classical correspondence formulation but more accurately represents the force state for each individual bond.

With the derived force state in Eqn. (29), the motion of a material point $\mathbf{X}$ in the reference configuration at time t is governed by

$$\rho\left(\mathbf{X}\right)\ddot{\mathbf{u}}\left(\mathbf{X}, t\right) = \int_{H_{\mathbf{X}}} \underline{\mathbf{T}}\left[\mathbf{X}, t\right]\langle\xi\rangle - \underline{\mathbf{T}}\left[\mathbf{X}', t\right]\langle -\xi\rangle \, dV_{\mathbf{X}'} + \mathbf{b}\left(\mathbf{X}, t\right)$$
$$\forall\left(\mathbf{X}, t\right) \in \Omega_r \times \left(0, T\right) \tag{30}$$

where $\rho\left(\mathbf{X}\right)$ is mass density, $\mathbf{u}\left(\mathbf{X}, t\right)$ is the displacement vector, $\underline{\mathbf{T}}\left[\mathbf{X}, t\right]$ is the force vector state that material point $\mathbf{X}'$ exerts on material point $\mathbf{X}$, and $\underline{\mathbf{T}}\left[\mathbf{X}', t\right]$ is the force vector state that material point $\mathbf{X}$ exerts on material point $\mathbf{X}'$, and $\mathbf{b}\left(\mathbf{X}, t\right)$ is external force density vector.

It's noteworthy that the proposed correspondence material model has the same properties, such as objectivity and balance of angular momentum, as conventional model since it recovers the conventional model when the size of bond-associated horizon greater than two times of the material point's horizon. See Fig. 5 for the case when $m' = 6.0$. The difference between the proposed model and conventional model lies in which neighbors are used in the force state calculation for each individual bond.

4. Parametric study

4.1. Selection of bond-associated horizon size

The size of the bond-associated horizon $h_{\mathbf{x}'}$ can be represented similarly to $H_{\mathbf{x}}$ in Eqn. (7), in terms of the mesh spacing Δx and a spacing factor m' for the bond-associated deformation gradient

$$\delta' = m' \cdot \Delta x \tag{31}$$

Changing m' results in a different configuration for the calculation of the bond-associated deformation gradient. To illustrate the effect of the choice of m' on the set of points involved in the bond-associated gradient calculation, a set of two-dimensional configurations with varying values of m' using regular spatial discretization are shown in Fig. 5. The classical correspondence configuration for deformation gradient is recovered for cases in which $m' \geq 2m$, as illustrated for the $m' = 6.0$ case. Further increasing m' beyond $2m$ clearly has no effect on the model.

It should be noted that for the bond-associated shape tensor and deformation gradient to be invertible, i.e., nonsingular, there must be at least two non-collinear bonds involved in the bond-associated gradient calculation. To satisfy this condition, the minimum value for m' is $\sqrt{2}$ for a regular grid. As can be seen from Fig. 5, the case of $m' = 1.0$ violates this condition. In that case, there are two bonds: one between point $\mathbf{X}$ (red) and material point $\mathbf{X}'$ (green), and one between point $\mathbf{X}$ and the one point shown in blue. Those two bonds are collinear, which results in a singular shape tensor and deformation gradient.

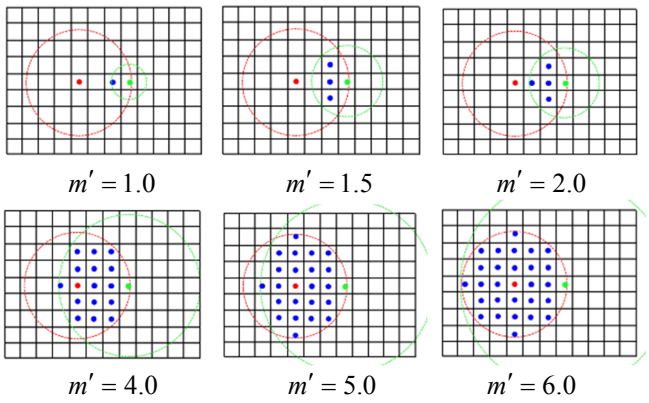

Fig. 5. Schematic diagrams of 2D configurations with constant horizon $m = 3$, but varying m'. Blue points are those used in the bond-associated deformation gradient calculation at material points $\mathbf{X}$ (red) for bond connecting with $\mathbf{X}'$ (green).

4. Numerical results

The proposed correspondence formulation was implemented based on the Multi-physics Object-Oriented Simulation Environment (MOOSE) framework [11] at Idaho National Laboratory. Some implicit formulation for peridynamic and other nonlocal discrete models can be found at [12] and [13]. Using this MOOSE-based implicit implementation, a parametric study on the effect of the size of bond-associated horizon is performed on a two-dimensional plate containing a center crack. A schematic showing the geometry and loading of the plate is given in Fig. 6. Pre-existing sharp cracks are

represented by removing connecting bonds between material points on each side of the crack surfaces. Boundary conditions are applied to only the first layers of material points adjacent to the edge of the model. The material properties are: Young's modulus $E = 210\ GPa$ and Poisson's ratio $v = 0.3$.

The mesh spacing used in this case is $\Delta x = 0.25\ mm$, which results in a total of 64,000 material points, and 40 material points on the crack surface. In this study, the standard peridynamic horizon is kept fixed with horizon spacing factor $m = 3.0$. Systematic comparisons on a number of different measures between different bond-associated configurations are performed. Comparison results for various values of m' under uniform normal traction of $10^9\ N/m^2$ force boundary condition are presented in Fig. 7. It is useful to refer to Fig. 5, which shows the effect of m' on the bond-associated deformation gradient calculation for many of the scenarios considered here. Note that the largest value of m' considered here is 5.0, because setting it to 6.0 or larger recovers the behavior of the classical correspondence model, which requires stabilization to yield reasonable results. A prediction comparison between the conventional model and proposed model is shown in Fig. 8 in terms of measures used in Fig. 7.

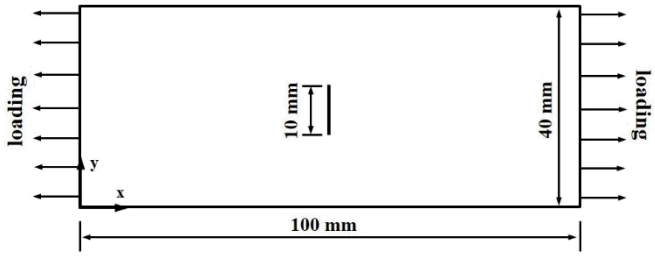

Fig. 6. Schematic showing geometry and configuration of a two-dimensional plate with pre-existing sharp crack

As can be seen from Fig. 7, all five peridynamic models produce smooth results except the case of $m' = 1.5$, which exhibits severe oscillation at the crack surfaces. This is due to the fact that a small bond-associated horizon size causes large fluctuations between approximated bond-associated state quantities for adjacent bonds. It also notable that the cases with smaller bond-associated horizon sizes show greater differences relative to the reference finite element method solution, but as m' increases, these differences decrease. For the case of $m' = 5.0$, the predictions align quite well with the finite element reference solution, considering the differences in geometrical representation of cracks between peridynamic models and finite element models. It's also evident that the peak values of strains and stresses at crack tips from peridynamic solution are much lower than those of the finite element reference solutions due to the non-locality in peridynamic models. It should be noted that the mesh used for the finite element model comparison had the same density as the peridynamic discretization.

From the simulations of the center-cracked plate, it can be concluded that for accuracy, the bond-oriented horizon size $h_{x'}$ needs to be no less than the horizon size H_x but smaller than two times of H_x, i.e., $m \le m' < 2m$.

From results shown in Fig. 8, there exists severe material instability, i.e., zero-energy modes, indicated as oscillation of the solutions in the conventional model. And the proposed formulation effectively removes this material instability.

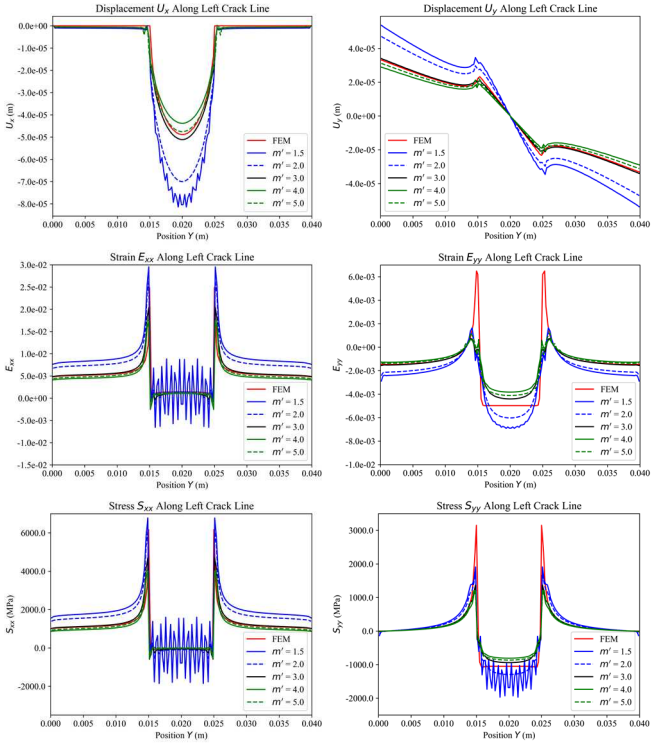

Fig. 7. Two-dimensional simulation results along a vertical line on the side of the crack for various bond-associated horizon sizes with force boundary conditions

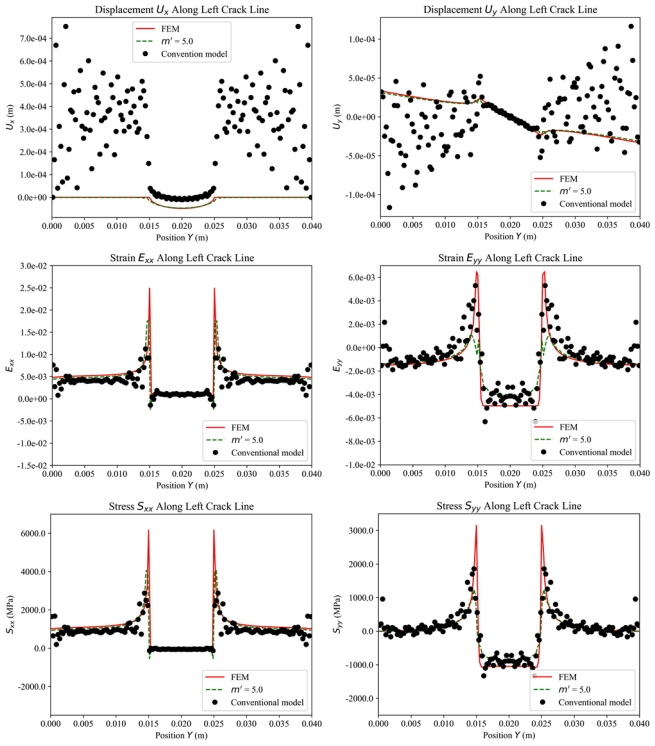

Fig. 8. Predictions comparison between proposed model and conventional model

5. Discussion and conclusion

Bond-associated deformation gradients were proposed to remove material instability in conventional correspondence model. A bond-associated deformation gradient is calculated from deformation states of materials points within each individual bond's proximity. Parametric study on the local horizon configuration for bond-associated quantities approximations suggested an optimal value for the bond-associated horizon size. A bond-oriented horizon size needs to be no less than the horizon size of the material point but smaller than two times of that value. The validity and accuracy of the proposed formulation was established by comparison of prediction against reference solution using finite element method.

The proposed formulation inherently resolves the material instability issue in conventional correspondence model, and has advantages over other zero-energy mode control methods in the literature at least in the following aspects:

1). The proposed formulation doesn't introduce any fictitious force states in addition to the original force states, which avoids utilization of zero-energy control parameters that must be tuned.

2). Compared to the stabilization methods introduced by Wu and Ren [6] and Yaghoobi and Chorzepa [8], the proposed formulation is shown to be far more effective at removing oscillations in stresses and strains near boundaries and at locations of local stress concentrations.

3). The proposed formulation is similar to the stabilization scheme recently proposed by Silling in Ref. [3], in that both of these methods minimize the non-uniform deformation state.

Acknowledgement

Work supported through the INL Laboratory Directed Research & Development (LDRD) Program under DOE Idaho Operation Office Contract DE-AC07-05ID14517. This manuscript has been authored by Battelle Energy Alliance, LLC under Contract No. DE-AC07-05ID14517 with the U.S. Department of Energy. The United States Government retains and the publisher, by accepting the article for publication, acknowledges that the United States Government retains a nonexclusive, paid-up, irrevocable, world-wide license to publish or reproduce the published form of this manuscript, or allow others to do so, for United States Government purposes.

References

1. Bobaru, F., et al., *Handbook of Peridynamic Modeling*. 2016, Boca Raton, FL: CRC Press.
2. Silling, S.A., et al., *Peridynamic States and Constitutive Modeling.* Journal of Elasticity, 2007. **88**(2): p. 151-184.
3. Silling, S.A., *Stability of peridynamic correspondence material models and their particle discretizations.* Computer Methods in Applied Mechanics and Engineering, 2017. **322**: p. 42-57.
4. Littlewood, D.J., *Simulation of Dynamic Fracture Using Peridynamics, Finite Element Modeling, and Contact.* Proceedings of ASME 2010 International Mechanical Engineering Congress and Exposition, 2010. **9**(44465): p. 209-217.
5. Breitenfeld, M.S., et al., *Non-ordinary state-based peridynamic analysis of stationary crack problems.* Computer Methods in Applied Mechanics and Engineering, 2014. **272**: p. 233-250.
6. Wu, C.T. and B. Ren, *A stabilized non-ordinary state-based peridynamics for the nonlocal ductile material failure analysis in metal machining process.* Computer Methods in Applied Mechanics and Engineering, 2015. **291**: p. 197-215.
7. Tupek, M.R. and R. Radovitzky, *An extended constitutive correspondence formulation of peridynamics based on nonlinear bond-strain measures.* Journal of the Mechanics and Physics of Solids, 2014. **65**: p. 82-92.
8. Yaghoobi, A. and M.G. Chorzepa, *Higher-order approximation to suppress the zero-energy mode in non-ordinary state-based peridynamics.* Computers & Structures, 2017. **188**: p. 63-79.
9. Gullett, P.M., et al., *A deformation gradient tensor and strain tensors for atomistic simulations.* Modelling and Simulation in Materials Science and Engineering, 2008. **16**(1): p. 015001.
10. Zimmerman, J.A., D.J. Bammann, and H. Gao, *Deformation gradients for continuum mechanical analysis of atomistic simulations.* International Journal of Solids and Structures, 2009. **46**(2): p. 238-253.
11. Gaston, D., et al., *MOOSE: A parallel computational framework for coupled systems of nonlinear equations.* Nuclear Engineering and Design, 2009. **239**(10): p. 1768-1778.
12. Chen, H., Y. Hu, and B.W. Spencer. *A MOOSE-Based Implicit Peridynamic Thermo-Mechanical Model*. in *ASME 2016 International Mechanical Engineering Congress and Exposition*. 2016. Phoenix, AZ.
13. Chen, H. and Y. Liu, *A non-local 3D lattice particle framework for elastic solids.* International Journal of Solids and Structures, 2016. **81**: p. 411-420.